STEM CELLS TRANSLATIONAL MEDICINE®

TISSUE-SPECIFIC PROGENITOR AND STEM CELLS

# Mesenchymal Stem Cell-Derived Exosomes Promote Fracture Healing in a Mouse Model

TAISUKE FURUTA,[a,*] SHIGERU MIYAKI,[a,b,*] HIROYUKI ISHITOBI,[b] TOSHIHIKO OGURA,[c] YOSHIO KATO,[c] NAOSUKE KAMEI,[a,b] KENJI MIYADO,[d] YUKIHITO HIGASHI,[b] MITSUO OCHI[a]

**Key Words.** Fracture healing • Mesenchymal stem cells • Exosomes • Endochondral ossification • Cytokine • microRNA

## ABSTRACT

**Paracrine signaling by bone-marrow-derived mesenchymal stem cells (MSCs) plays a major role in tissue repair. Although the production of regulatory cytokines by MSC transplantation is a critical modulator of tissue regeneration, we focused on exosomes, which are extracellular vesicles that contain proteins and nucleic acids, as a novel additional modulator of cell-to-cell communication and tissue regeneration. To address this, we used radiologic imaging, histological examination, and immunohistochemical analysis to evaluate the role of exosomes isolated from MSC-conditioned medium (CM) in the healing process in a femur fracture model of CD9$^{-/-}$ mice, a strain that is known to produce reduced levels of exosomes. We found that the bone union rate in CD9$^{-/-}$ mice was significantly lower than wild-type mice because of the retardation of callus formation. The retardation of fracture healing in CD9$^{-/-}$ mice was rescued by the injection of exosomes, but this was not the case after the injection of exosomes-free conditioned medium (CM-Exo). The levels of the bone repair-related cytokines, monocyte chemotactic protein-1 (MCP-1), MCP-3, and stromal cell-derived factor-1 in exosomes were low compared with levels in CM and CM-Exo, suggesting that bone repair may be in part mediated by other exosome components, such as microRNAs. These results suggest that exosomes in CM facilitate the acceleration of fracture healing, and we conclude that exosomes are a novel factor of MSC paracrine signaling with an important role in the tissue repair process.** STEM CELLS TRANSLATIONAL MEDICINE *2016;5:1620–1630*

## SIGNIFICANCE

This work focuses on exosomes, which are extracellular vesicles, as a novel additional modulator of cell-to-cell communication. This study evaluated the role of exosomes isolated from mesenchymal stem cell (MSC)-conditioned medium (MSC-CM) in the fracture-healing process of CD9$^{-/-}$ mice, a strain that is known to produce reduced levels of exosomes. Retardation of fracture healing in CD9$^{-/-}$ mice was rescued by the injection of MSC exosomes, but this was not the case after the injection of exosome-free CM. This study finds that MSC exosomes are a novel factor of MSC paracrine signaling, with an important role in the tissue repair process.

## INTRODUCTION

Poor or impaired recovery from fractures is an increasingly important problem in aging societies. Although most fractures are repaired through intramembranous ossification and endochondral ossification, in approximately 10% of cases, union is delayed or compromised because of impaired blood supply and recruitment of homing stem cells, excessive damage to the periosteum, inadequate immobilization, or infection at the injury site [1]. Although autologous bone transplantation and vascularized bone grafts have been performed for delayed-union or nonunion fractures [2], current therapies are often ineffective. An improved understanding of the molecular mechanisms underlying bone repair is needed to inform the development of new therapies for patients with delayed-union or nonunion complications from fractures.

Transplantation of stem cells, such as bone-marrow-derived mesenchymal stem cells (MSCs), promotes tissue regeneration, including fracture healing [3–5]. Many studies indicate that transplanted MSCs contribute to tissue regeneration by mechanisms other than differentiation and direct tissue integration [6–9]. Therefore, paracrine signaling by MSCs is attracting attention as a potential mechanism to explain the effect of these cells on tissue regeneration. The paracrine effect is mediated by proteins such as cytokines and chemokines with antiapoptotic, anti-inflammatory, antioxidative, and

[a]Department of Orthopaedics Surgery, Integrated Health Sciences, Institute of Biomedical and Health Science, Hiroshima University, Hiroshima, Japan; [b]Department of Regenerative Medicine, Medical Center for Translational and Clinical Research, Hiroshima University Hospital, Hiroshima, Japan; [c]Biomedical Research Institute, National Institute of Advanced Industrial Science and Technology, Tsukuba, Japan; [d]Department of Reproductive Biology, National Center for Child Health and Development, Tokyo, Japan

[*]Contributed equally.

Correspondence: Taisuke Furuta, M.D., Department of Orthopaedics Surgery, Integrated Health Sciences, Institute of Biomedical and Health Science, Hiroshima University, 1-2-3 Kasumi, Minami-ku, Hiroshima, 734-5234, Japan. Telephone: 81-82-257-5233; E-Mail: fu09100913@yahoo.co.jp

Received November 2, 2015; accepted for publication June 28, 2016; published Online First on July 26, 2016.


1066-5099/2016/$20.00/0

http://dx.doi.org/10.5966/sctm.2015-0285

proangiogenic properties [10]. MSC-conditioned medium accelerates callus formation, and monocyte chemotactic protein-1 (MCP-1) and stromal cell-derived factor-1 (SDF-1) are essential in the initial phase of fracture healing by regulating the recruitment and differentiation of MSCs and other progenitor cells [11–14].

Recently, extracellular vesicles, including exosomes, have attracted increasing attention as mediators of cell-to-cell communication [15, 16]. Exosomes are small particles of 30–200 nm that are derived from the fusion of multivesicular bodies to plasma membranes, and they are secreted into the extracellular environment by most cells. Tetraspanins, such as CD9 and CD81, are characteristic markers and membranous components of exosomes [17–21]. CD9 is a transmembrane protein associated with angiogenesis via cell adhesion, migration, and signal transduction, and it is involved in cell fusion processes linked to fertilization, osteoclastogenesis, and myogenesis [22–30]. Eggs and dendritic cells from CD9-deficient mice release reduced levels of exosomes [31, 32]. Recent studies have shown that extracellular vesicles, such as exosomes derived from MSCs, mediate regenerative functions in several diseases, including those affecting the kidney and heart [33–35]. We also reported that MSC-derived exosomes promote muscle regeneration by enhancing myogenesis and angiogenesis [36]. Although the paracrine effect of MSCs has been suggested to be the major mechanism driving tissue regeneration after MSC transplantation, the paracrine factors produced by MSCs have not been completely defined. The objective of this study was to address the function of MSC-derived exosomes as novel paracrine factors in fracture healing by using a mouse model of fracture.

## Materials and Methods

### Animals

C57BL/6 wild-type mice were obtained from CLEA Japan Inc. (Tokyo, Japan, http://www.clea-japan.com). $CD9^{-/-}$ mice on a C57BL/6 background were described previously [28] and were bred in our institution. This study was reviewed and approved by the Ethics Committee for Experimental Animals of Hiroshima University, and all animals were treated according to the guidelines of the Institutional Animal Care and Use Committee.

### Fracture Model

The fracture model involved 77 male mice between 17 and 19 weeks old. A transverse femoral shaft fracture was generated by using a C-shaped instrument applying three-point bending. The right knee was exposed by using the lateral parapatellar approach with the patella medially dislocated. The femur intercondylar groove was exposed at the knee joint by full flexion, and a burr hole of 0.5-mm diameter was made in the center of the intercondylar groove. To avoid significant displacement of the fracture while maintaining a well-aligned and stable fracture site, a 0.5-mm-diameter 24-gauge needle was inserted into the burr hole at the center of the intercondylar groove, and the tip of the needle was run through the top of the femur greater trochanter. A thin saw cut at a depth of 3 mm was applied midshaft after minimal lateral exposure to weaken the bone and to avoid complex fractures. The right femur of each animal was fractured by a three-point bending technique [3, 37], after which the muscular fasciae and skin were closed.

### Radiologic Analysis for Bone Union

X-ray and microcomputed tomography ($\mu$CT) imaging were performed by using a high-resolution Skyscan 1176 in-vivo micro-CT (Bruker, Madison, WI, https://www.bruker.com). Three-dimensional CT images were recreated by CTAn (version 1.15) + CTVol (version 2.3) software (Bruker). The bone densities of the femur shafts of wild-type mice ($n$ = 10) and $CD9^{-/-}$ mice ($n$ = 10) were measured by computed tomography using CTAn (version 1.15) + CTVol (version 2.3) software (Bruker). Radiographic imaging was performed at 0, 1, 2, 4, and 6 weeks after fracture. Bone union was defined as the presence of a bridging callus on two cortices [3].

### Histological Evaluation

The femurs of 1-month-old wild-type and $CD9^{-/-}$ mice were harvested at 3 and 10 days after fracture. These samples were embedded in paraffin after fixation in 4% paraformaldehyde at 4°C for 24 hours and decalcification in 10% EDTA (Wako, Osaka, Japan, http://www.wako-chem.co.jp) at room temperature for 14 days. The femurs were sectioned (4.5-$\mu$m slices) along the longitudinal axis with a microtome and stained with Toluidine blue (Sigma-Aldrich, St. Louis, MO, http://www.sigmaaldrich.com), hematoxylin and eosin (H&E) (Sigma-Aldrich), and tartrate-resistant acid phosphatase (TRAP) (Wako) for analysis of histologic differences. At least two different sections per sample were analyzed microscopically. Fracture healing was evaluated by using a histological score of fracture healing [38]. TRAP-positive cells' $mm^2$ field was counted.

### Immunohistochemical Analysis

Sections from paraffin-embedded femur were first deparaffinized in xylene and rehydrated in ethanol and water. After washing with PBS, sections were blocked with 10% serum for 20 min at room temperature. Antibodies to $\alpha$-smooth muscle actin ($\alpha$SM) (Abcam, Austin, TX, http://www.abcam.com; ab5694; 1:200) were added and incubated overnight at 4°C. After washing with phosphate-buffered saline (PBS), sections were incubated with biotinylated secondary antibody for 30 minutes at room temperature and then incubated with Vectastain ABC-AP alkaline phosphatase (Vector Laboratories, Burlingame, CA, http://vectorlabs.com) for 30 min. Slides were washed, and sections were incubated with alkaline phosphatase substrate (Vector Laboratories).

### Preparation of Conditioned Medium and Isolation of Exosomes

Human bone marrow-derived MSCs (MSCs) were obtained from Lonza (Basel, Switzerland, http://www.lonza.com) and cultured in MSC growth medium (Lonza). The human osteosarcoma cell line HOS was obtained from the American Type Culture Collection and maintained in Dulbecco's Modified Eagle's Medium (DMEM; Wako) with 10% fetal bovine serum and 1% antibiotic-antimycotic solution (Nacalai Tesque, Kyoto, Japan, http://www.nacalai.co.jp). The MSCs were cultured at 37°C under 5% $CO_2$, and MSCs at passages 4–6 were used for all experiments. MSCs were seeded at $1.0 \times 10^5$ per well in a six-well plate with MSC growth medium. One day later, the cells were washed with serum-free DMEM and cultured with 2 ml/well serum-free DMEM for 48 hours. To isolate the exosomes,

 

2 ml of conditioned medium (CM) was collected and centrifuged for 15 minutes at 2,380*g* and then further ultracentrifuged for 70 minutes at 180,000*g* at 4°C. The supernatants were collected as exosome-depleted conditioned medium (CM-Exo). The exosome pellets were resuspended in 100 $\mu$l of PBS. The exosomes isolated from the same volumes of culture medium and from the same numbers of cells were resuspended in PBS or DMEM. CM and CM-Exo were concentrated by using Amicon Ultra-2 centrifugal filters (EMD Millipore, Billerica, MA, http://www.emdmillipore.com), according to the recommended protocol. For local injection into a femur fracture model of CD9$^{-/-}$ or wild-type mice, 100 $\mu$l of exosomes, CM, or CM-Exo was injected into the fractured part at 1 and 8 days after fracture.

### Immunoblotting of Exosome Markers

Proteins from CM, CM-Exo, and exosomes were separated on Mini-Protean TGX Precast Gels (Bio-Rad Laboratories, Hercules, CA, http://www.bio-rad.com) and transferred to a poly(vinylidene) difluoride membrane (Bio-Rad Laboratories). Antiflotillin-1 antibody (610820; diluted 1:500; BD Biosciences, San Jose, CA, http://www.bdbiosciences.com; purified), mouse anti-human CD9 antibody (BD Bioscience; diluted 1:200), and anti-CD81 antibody (Santa Cruz Biotechnology, Dallas, TX, http://www.scbt.com; sc-7637; diluted 1:200) were used as primary antibodies. Horseradish peroxidase (HRP)-conjugated goat anti-mouse IgG antibody (Santa Cruz Biotechnology; diluted sc-2005) or HRP-conjugated goat anti-rabbit IgG antibody (Santa Cruz Biotechnology; sc-2030) were used as the secondary antibodies. The signal was detected by chemiluminescence with immuno-enhancer (Wako) by using the ImageQuant LAS 4000 system (GE Healthcare, Uppsala, Sweden, http://www3.gehealthcare.co.jp).

### The High-Resolution Frequency Transmission Electric-Field System

We recently developed a high-resolution frequency transmission electric-field (FTE) imaging system based on field emission scanning electron microscopy (SEM) of JSM-7000F (JEOL, Tokyo, Japan, http://www.jeol.co.jp), which enables observation of the biological specimens in water without metal staining [39]. Exosomes were imaged by using the FTE imaging system. The observation conditions were captured under the following parameters: $\times$20,000 magnifications, 1,280 $\times$ 1,024 pixels, 80-second scanning time, 7-mm working distance, 3- to 4-kV accelerating EB, and 10-pA current. Original FTE images were filtered by using a two-dimensional Gaussian filter (GF) with the kernel size of 7 $\times$ 7 pixels and the radius of 1.2$\sigma$. Background subtraction was achieved by subtracting FTE images from the filtered images using a broad GF (400 $\times$ 400 pixels, 160$\sigma$).

### Cytokine/Growth Factor Assay

Profiling of angiogenesis-related proteins (55 proteins) and cytokines (102 proteins) in CM, CM-Exo, and exosomes was undertaken by using a Human Angiogenesis Array kit and a Human XL Cytokine Antibody Array kit (Proteome Profiler, R&D Systems, Minneapolis, MN, https://www.rndsystems.com), according to the recommended protocols. The concentrations of monocyte chemotactic protein-1 (MCP-1), MCP-3, and stromal cell-derived factor-1 (SDF-1) in the CM, CM-Exo, and exosomes from MSCs and HOS were quantified by using the Bio-Plex Multiplex suspension assay system (Bio-Rad Laboratories), according to the recommended protocol.

### Nanostring nCounter microRNA Analysis

Small RNAs were purified from MSC and HOS exosomes by using the mirVana miRNA Isolation Kit (Thermo Fisher Scientific Life Sciences, Oakwood Village, OH, https://www.thermofisher.com). Purified small RNAs were concentrated by using an evaporator. The concentrations and quality of the small RNAs from the same volumes of culture medium for the same numbers of cells were determined with the Bio-Analyzer 2100 (Agilent Technologies, Santa Clara, CA, http://www.agilent.com), and small RNA was used as the input for the nCounter Human miRNA Expression Assay Kit (NanoString Technologies, Seattle, WA, http://www.nanostring.com) as described previously [36].

### Statistical Analysis

All quantitative data are expressed as mean $\pm$ SD. Statistical analyses were performed by Pearson's chi-square test, the Mann-Whitney *U* test, or the Steel-Dwass test. A value of $p < .05$ was considered statistically significant.

## Results

### Fracture Healing in Wild-Type and CD9$^{-/-}$ Mice

Skeletal development in CD9$^{-/-}$ mice was normal. Body weight, bone density, and the entire width of the tibial growth plate were measured in wild-type and CD9$^{-/-}$ mice. Body weight and bone density were not significantly different between wild-type and CD9$^{-/-}$ mice at 17 weeks old, just before fracture (Fig. 1A, 1B). Furthermore, to confirm whether there was an inherent difference in bone growth, we measured the width of the tibial growth plates in wild-type and CD9$^{-/-}$ mice at 1 month old. The widths of the tibial growth plates were significantly reduced in CD9$^{-/-}$ mice compared with wild-type mice (Fig. 1C). Next, we examined the process of fracture healing in CD9$^{-/-}$ mice. Wild-type mice exhibited endochondral ossification through callus formation 2 weeks after fracture, and bone union was apparent at 3 weeks (Fig. 2A). However, CD9$^{-/-}$ mice showed a significant delay in fracture healing compared with wild-type mice. Bone union rate was 25% in CD9$^{-/-}$ mice at 3 weeks after fracture, which was significantly lower than wild-type mice (Fig. 2B). The average period for bone union in CD9$^{-/-}$ mice was also significantly longer than wild-type mice (data not shown). Histological analyses of the fracture revealed that endochondral ossification was particularly delayed in CD9$^{-/-}$ mice compared with wild-type mice (Fig. 2C) at 2 and 3 weeks after the fracture. Overall, these results showed that healing capacity was decreased in CD9$^{-/-}$ mice compared with wild-type mice.

### MSC Exosomes Rescued Delayed Fracture Healing in CD9$^{-/-}$ Mice

We examined whether delayed fracture healing in CD9$^{-/-}$ mice was rescued by injection of MSC-derived exosomes. Exosomes were isolated from MSC-conditioned medium by ultracentrifugation (Fig. 3A). Exosome markers CD9, CD81, and flotillin-1 were examined in

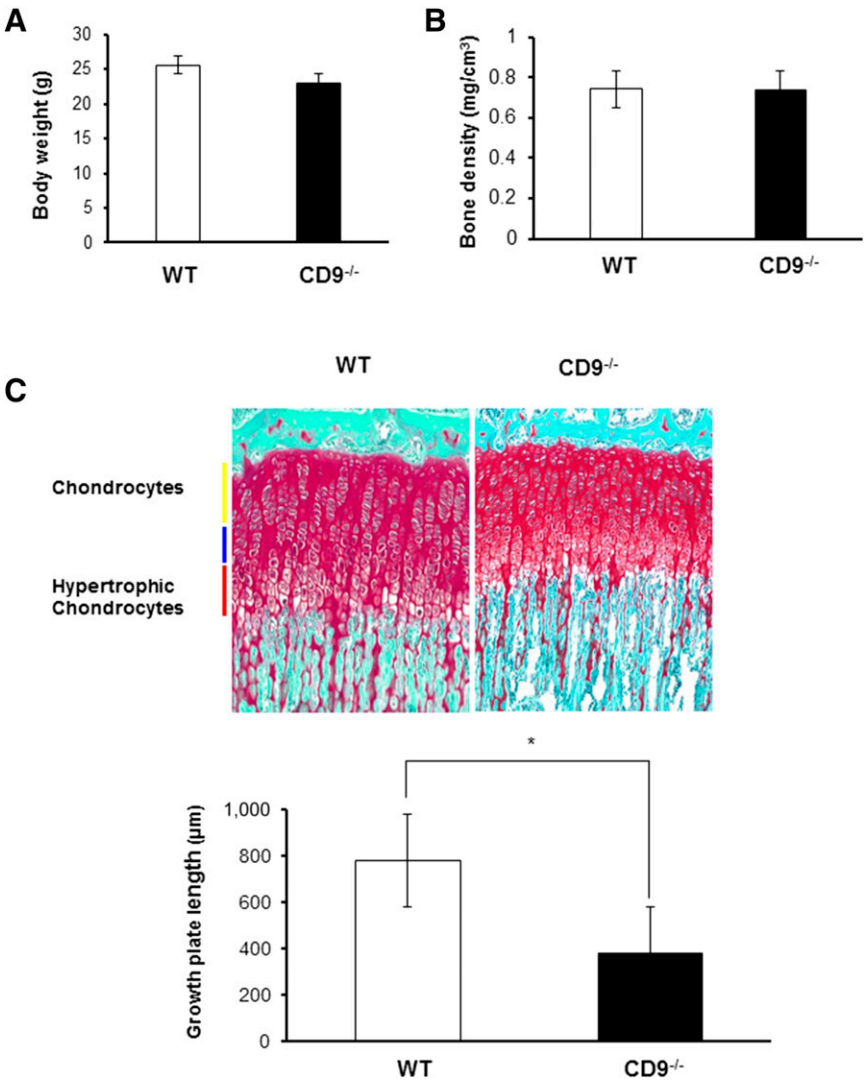


**Figure 1.** Body weight, bone density, and the entire width of the tibial growth plate in CD9$^{-/-}$ mice. **(A, B):** The body weight and bone density were measured in WT ($n$ = 10) and CD9$^{-/-}$ ($n$ = 10) mice at 17 weeks old, just before fracture. **(C):** The tibial growth plate length was measured in WT and CD9$^{-/-}$ mice at 1 month old. Growth plate lengths in CD9$^{-/-}$ mice were significantly shorter than those in WT. Scale bars = 200 $\mu$m. Values were expressed as means $\pm$ SE. Statistical analysis was performed by Mann-Whitney $U$ test. $*$, $p < .05$. Abbreviation: WT, wild-type mice.

the conditioned medium (CM), supernatant (CM-Exo), and exosome pellet after ultracentrifugation by immunoblotting. Exosome markers were detected in the CM and exosome preparations, but not in the CM-Exo, after ultracentrifugation (Fig. 3B). The FTE imaging system was directly able to image the untreated exosomes in solution. These exosome images clearly showed a spherical shape of approximately 80 nm (Fig. 3C). The CM-Exo was less than exosome preparations (Fig. 3C).

To examine the effect of exosomes on fracture healing in CD9$^{-/-}$ mice, 100 $\mu$l of CM, CM-Exo, or exosomes were injected into the fracture site. Delayed fracture healing in CD9$^{-/-}$ mice was rescued by the injection of CM and exosomes (Fig. 4A). The injection of CM and exosomes was associated with abundant callus formation 2 weeks after fracture; bone union at 3 weeks after fracture was similar to wild-type mice. However, delayed fracture healing in CD9$^{-/-}$ mice was not rescued by CM-Exo (Fig. 4A). The average period for bone union was significantly different between MSC exosome-treated and CM Exo-treated or control groups (Fig. 4B). These results indicated that exosomes rescued delayed fracture healing in CD9$^{-/-}$ mice. Histological analysis with toluidine blue and H&E staining revealed that there was accelerated formation of hypertrophic chondrocytes and woven bone in the exosome-injected CD9$^{-/-}$ mice, and there was significant improvement in fracture healing in exosome-injected CD9$^{-/-}$ mice compared with PBS-injected control CD9$^{-/-}$ mice (Fig. 4C, 4D). Indeed, many TRAP-positive cells were present in the calluses of exosome-injected CD9$^{-/-}$ mice 10 days after surgery, whereas very few TRAP-positive cells were detected in the calluses of control mice (Fig. 4D). Cells positive for the vascular marker $\alpha$SM were also increased in calluses of exosome-injected CD9$^{-/-}$ mice, in contrast to calluses of PBS-injected CD9$^{-/-}$ mice (Fig. 4D). Overall, these data are consistent with supplementing exosomes facilitating an improved fracture healing process in CD9$^{-/-}$ mice. Furthermore, to examine whether the

 

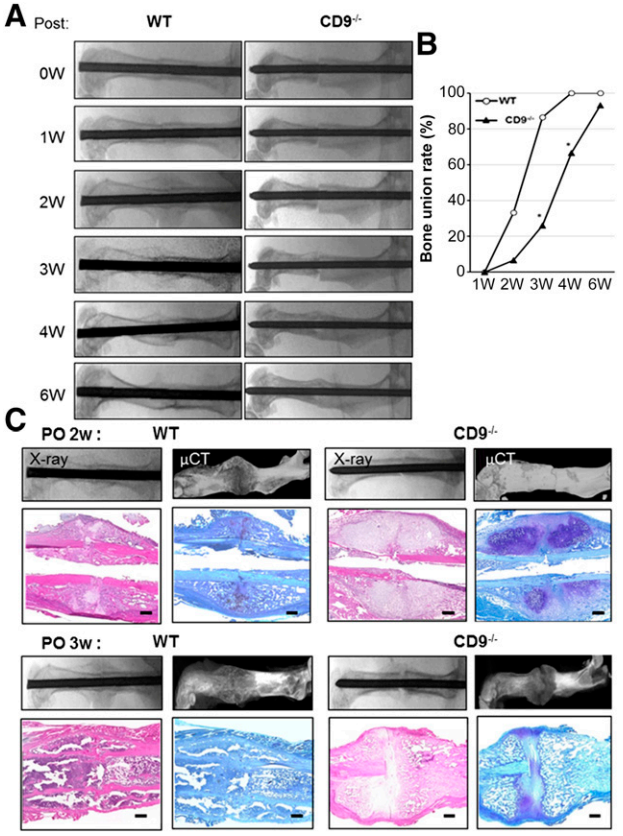


**Figure 2.** Impaired fracture healing in CD9$^{-/-}$ mice. **(A, B):** A transverse femoral shaft fracture was produced by using a C-shaped instrument applying three-point bending in WT ($n$ = 15) and CD9$^{-/-}$ ($n$ = 15) mice. Radiographic imaging by x-ray and bone union rate were performed at 0, 1, 2, 4, and 6 weeks after the fracture. Statistical analysis was performed by Pearson's chi-square test. $*$, $p < .05$. **(C):** The femurs of WT and CD9$^{-/-}$ mice were harvested at 2 and 3 weeks after fracture. After radiographic imaging by x-ray and $\mu$CT was performed, the femurs were stained with Toluidine blue, and H&E. Scale bars = 100 $\mu$m. Abbreviations: $\mu$CT, microcomputed tomography; PO, postoperative; 0W, 0 weeks; WT, wild-type mice.

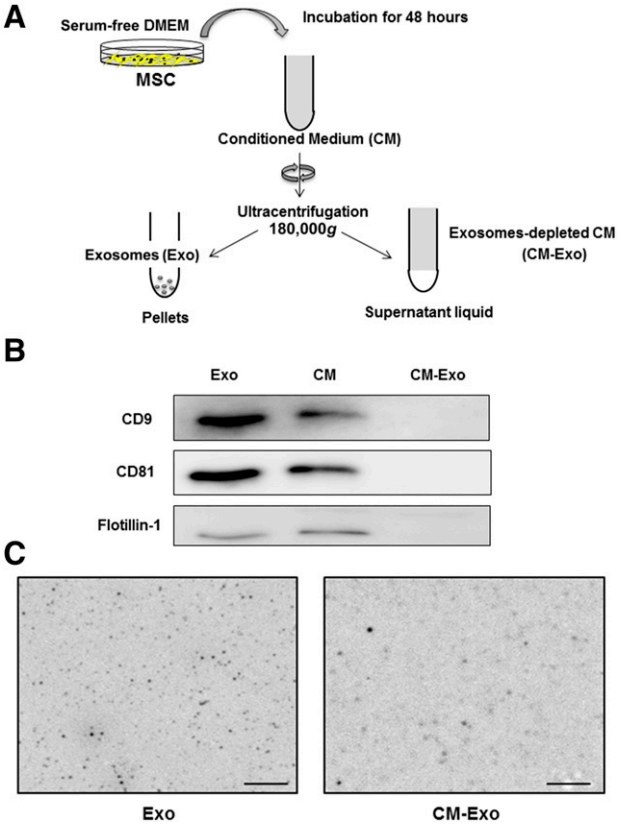


**Figure 3.** Isolation of exosomes from MSC-conditioned medium. **(A):** MSCs were seeded at $1.0 \times 10^5$ cells per well in a six-well plate with MSC growth medium. One day later, the cells were washed with serum-free DMEM and cultured with 2 ml per well serum-free DMEM for 48 hours. To isolate the exosomes, 2 ml of conditioned medium (CM) was collected and centrifuged for 15 minutes at 2,380$g$ and then further ultracentrifuged for 70 minutes at 180,000$g$. The supernatants were collected as exosome-depleted conditioned medium. The pellets were resuspended in PBS for use as exosomes. **(B):** Immunoblotting for exosome markers, CD9, CD81, and flotillin-1, in Exo, CM and CM-Exo. **(C):** Images of the untreated Exo and CM-Exo in solution by FTE system. Original magnification $\times$20,000. Scale bars = 1 $\mu$m. Abbreviations: CM, conditioned medium; CM-Exo, exosome-depleted conditioned medium; DMEM, Dulbecco's modified Eagle's medium; Exo, exosomes; MSC, mesenchymal stem cell; PBS, phosphate-buffered saline.

promotion of fracture healing by exosomes depends on MSC-derived exosomes specifically, exosomes collected from the human osteosarcoma cell line HOS were injected into fractured femurs of CD9$^{-/-}$ mice and compared with mice treated with MSC exosomes. Although MSC exosomes promoted callus formation at 10 days after the fracture, HOS exosomes failed to promote callus formation (Fig. 4E).

## MSC Exosomes Promote Fracture Healing in Wild-Type Mice

CM, CM-Exo, and MSC exosomes were injected into the fractured femurs of wild-type mice to examine whether exosomes promote fracture healing in the wild-type context. Although the injection of CM and exosomes promoted bone union at 2 weeks after fracture, bone union was not enhanced by CM-Exo in wild-type mice (Fig. 5A). The timing of bone union was significantly shorter in mice treated with CM and exosomes compared with the control and CM-Exo groups (Fig. 5B). These results indicated that exosomes promote fracture healing in wild-type mice.

## Cytokines and microRNAs in MSC Exosomes

Cytokine antibody arrays (102 proteins) and angiogenesis antibody arrays (55 proteins) were used to identify proteins that were present in CM, CM-Exo, and exosomes preparations. Interestingly, these assays revealed that the levels of cytokines and angiogenic factors such as vascular endothelial growth factor (VEGF) in MSC exosomes were lower than those in CM and CM-Exo (supplemental online Fig. 1A, 1B). To more accurately assess the concentrations of the cytokines, MCP-1, MCP-3, and SDF-1, all known to be essential for fracture healing [11–14], the levels of these factors in CM, CM-Exo, MSC exosomes, and HOS exosomes were quantified by using a Bio-Plex system (Fig. 5C). SDF-1, MCP-1, and MCP-3 levels in MSC exosomes were significantly lower than the levels in CM and CM-Exo (Fig. 5C).

To assay microRNAs (miRNAs) in MSC exosomes, we compared MSC exosomes with HOS exosomes using the NanoString

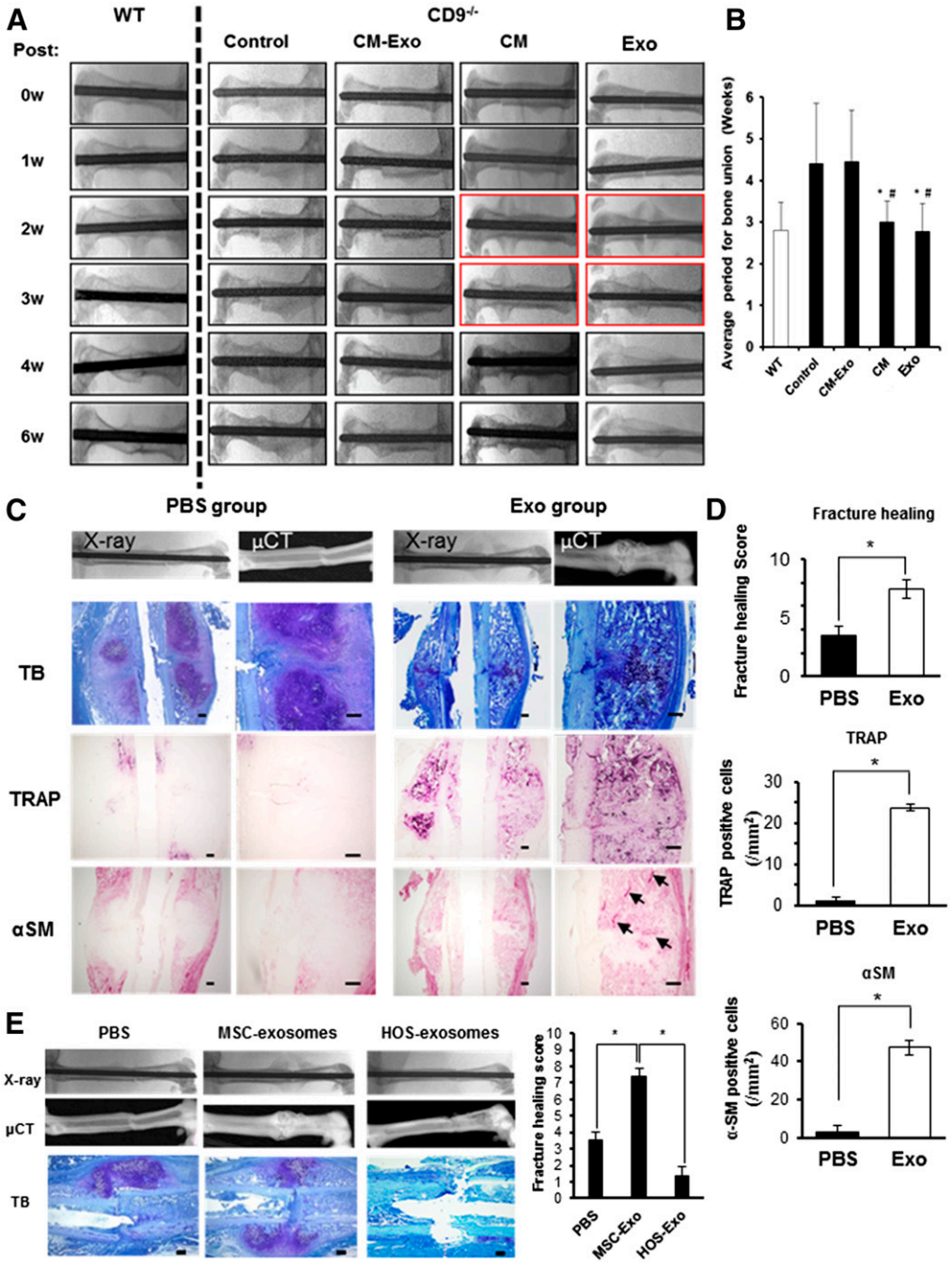


**Figure 4.** MSC exosomes rescued delayed fracture healing in CD9$^{-/-}$ mice. **(A):** Representative radiologic images of control ($n = 15$), CM ($n = 9$), CM-Exo ($n = 9$), and Exo ($n = 9$) treated CD9$^{-/-}$ mice at 0, 1, 2, 4, and 6 weeks after fracture. **(B):** The average period for bone union. Statistical analysis was performed by Steel-Dwass test. #, $p < .05$ versus control; ∗, $p < .05$ versus CM-Exo. **(C):** Representative histological evaluation of callus formation after Exo injection in CD9$^{-/-}$ mice. The femurs of PBS control and Exo-treated CD9$^{-/-}$ mice were assayed 10 days after fracture. The femurs were stained with Toluidine blue (PBS, $n = 6$; Exo, $n = 5$), TRAP (PBS, $n = 4$; Exo, $n = 4$), and $\alpha$SM antibody (PBS, $n = 4$; Exo, $n = 4$) for histologic analysis of callus. Scale bars = 200 $\mu$m (right column) and 100 $\mu$m (left column). **(D):** Quantification of fracture healing, osteoclasts (TRAP) and angiogenesis ($\alpha$SM) in calluses. Values were expressed as mean ± SE. Statistical analysis was performed by Mann-Whitney *U* test, ∗, $p < .05$. **(E):** Representative radiologic images and $\mu$CT images of femurs. The femurs of PBS-injected control CD9$^{-/-}$ mice, MSC-Exo-treated CD9$^{-/-}$ mice, and HOS-Exo-treated CD9$^{-/-}$ mice were harvested at 10 days after fracture. The femurs were stained with Toluidine blue (PBS, $n = 6$; MSC-Exo, $n = 5$; HOS-Exo, $n = 5$) for histologic analysis. Scale bars = 100 $\mu$m. Fracture healing scores were generated after histological evaluation. Statistical analysis was performed by Steel-Dwass test. ∗, $p < .05$. Control, no injection group. Abbreviations: CM, conditioned medium; CM-Exo, exosome-depleted conditioned medium; $\mu$CT, microcomputed tomography; Exo, exosomes; HOS, human osteosarcoma cells; MSC, mesenchymal stem cell; PBS, phosphate-buffered saline; $\alpha$SM, $\alpha$-smooth muscle actin; TB, Toluidine blue; TRAP, tartrate-resistant acid phosphatase; 0W, 0 weeks; WT, wild type.

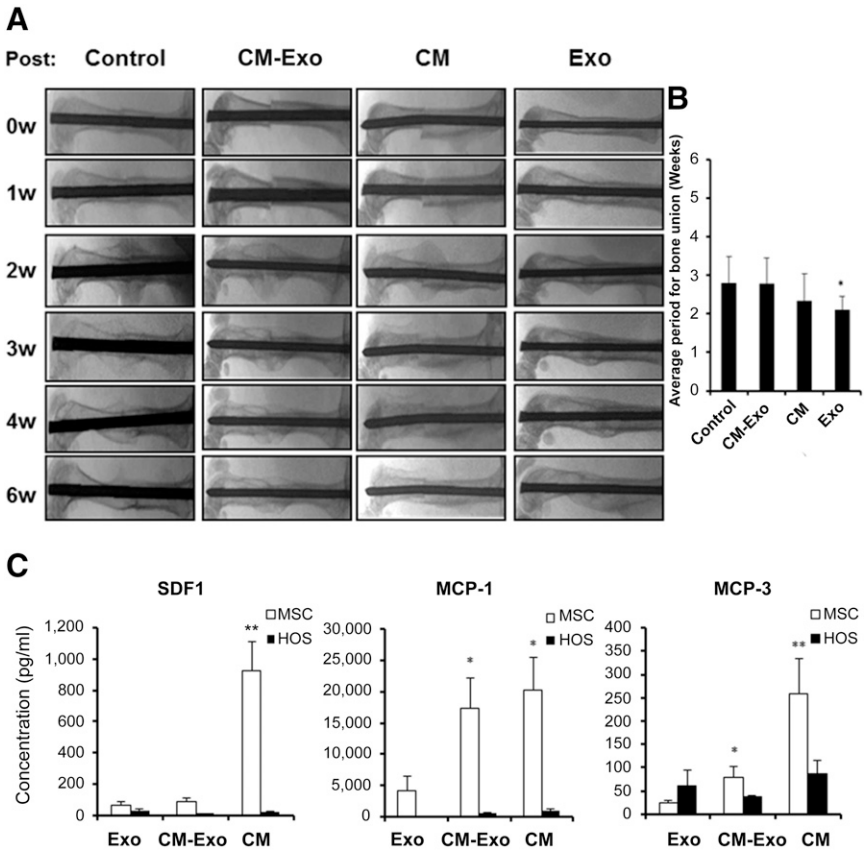


**Figure 5.** MSC exosomes promote fracture healing in wild-type mice. **(A):** Representative radiologic images of the femurs of control ($n = 15$), CM ($n = 9$), CM-Exo ($n = 9$), and Exo ($n = 9$) treated WT mice. **(B):** The average period for bone union. Statistical analysis was performed by Steel-Dwass test. $*$, $p < .05$ versus control. Control, no injection group. **(C):** The concentrations of the bone-repair-related cytokines, MCP-1, -3, and SDF-1 were measured in CM, exosomes, and CM-Exo from MSCs and HOS cells by using Bio-Plex assays. Some values in CM and CM-Exo from MSCs were used with 29,575.6 pg/ml as the maximum concentration within range, because the values of MCP-1 in CM and CM-Exo from MSCs were out of range of the standard curve. Values were expressed as mean ± SE. Statistical analysis was performed by Steel-Dwass test. $*$, $p < .05$ versus MSC-Exo; $**$, $p < .01$ versus MSC-Exo. hMSC was from nine donors ($n = 17$). Abbreviations: CM, conditioned medium; CM-Exo, exosome-depleted conditioned medium; Exo, exosomes; HOS, human osteosarcoma cells; MCP-1, monocyte chemotactic protein-1; MSC, mesenchymal stem cell; SDF-1, stromal cell-derived factor-1; 0w, 0 weeks.

system. We previously described the top 20 most highly expressed miRNAs in MSC exosomes and CM-Exo [36]. The top 30 most highly expressed miRNAs in MSC and HOS exosomes were very similar (Table 1). Differentially expressed miRNAs are shown as the ratio of miRNA expression level in MSC to HOS exosomes (Table 2). Of the top 10 listed in Table 2, miR-4532, miR-125b-5p, and miR-4516 also appeared in the top 30 most highly expressed miRNAs in MSC exosomes (Table 1). miR-338-3p and miR-548aa were expressed at more than threefold higher levels in MSC exosomes relative to CM-Exo.

## Discussion

Impaired tissue repair has been linked to compromised chemotaxis [24], vascularization [22, 23], and cell fusion [26] in $CD9^{-/-}$ mice [40–42]. In addition to these phenotypes, exosome release is reduced in these mice [31, 32]. Thus, we hypothesized that impaired fracture healing in $CD9^{-/-}$ mice may be linked to compromised exosome release compared with wild-type mice, and augmented fracture healing might be achieved in this mouse model by supplementing exosomes. In this study, there were no significant differences in weight and bone density between wild-type and $CD9^{-/-}$ mice at 17 weeks old. Although in vitro studies show that CD9 positively regulates osteoclastogenesis via cellular fusion and MAPK signaling [29, 30], osteoclast activity under the tibial growth plate is similar in wild-type and $CD9^{-/-}$ mice at 8 weeks old [43]. Similarly, there were also no obvious differences in osteogenesis between wild-type mice and CD9/CD81 double-knockout mice [43]. Thus, these data suggest that osteoclastogenesis and osteogenesis are normal in $CD9^{-/-}$ mice. However, our study revealed that the width of the tibial growth plate was significantly reduced in $CD9^{-/-}$ mice compared with wild-type mice at 1 month old. These results may indicate that the initial phase of endochondral ossification, including chondrocyte proliferation and hypertrophic differentiation, was impaired in this model system. Indeed, $CD9^{-/-}$ mice exhibited retardation of callus formation compared with wild-type mice. Furthermore, cell recruitment is known to be important in the initial phase of fracture healing. The expression of CD9 on stem cells, including $CD34^{+}$ hematopoietic stem cells, regulates migration, adhesion, and homing [44, 45]. Thus, the retardation of fracture healing in $CD9^{-/-}$ mice might be related to impaired homing of stem and progenitor cells to the fracture site. However, in our study, the expression of CD9 did

**Table 1.** Top 30 most highly expressed miRNAs in MSC exosomes and HOS exosomes according to NanoString miRNA expression profiling.

| | MSC exosomes | | HOS exosomes | |
|---|---|---|---|---|
| No. | miRNAs | Signal intensity | miRNAs | Signal intensity |
| 1 | **hsa-miR-21-5p** | 23,823 | **hsa-miR-4454** | 13,915.81 |
| 2 | **hsa-miR-125b-5p** | 11,785.5 | hsa-miR-1246 | 11,008.52 |
| 3 | **hsa-miR-4454** | 11,007.9 | **hsa-miR-21-5p** | 10,707.99 |
| 4 | **hsa-let-7a-5p** | 4,038.9 | **hsa-miR-29b-3p** | 5,612.06 |
| 5 | **hsa-miR-23a-3p** | 3,506.14 | **hsa-let-7a-5p** | 5,210.26 |
| 6 | **hsa-miR-378e** | 3,340.55 | **hsa-miR-23a-3p** | 2,930.16 |
| 7 | **hsa-miR-720** | 2,915.78 | hsa-miR-15b-5p | 2,835.43 |
| 8 | **hsa-miR-4286** | 2,915.78 | **hsa-miR-720** | 2,815.83 |
| 9 | **hsa-miR-4443** | 2,771.79 | **hsa-miR-125b-5p** | 2,547.97 |
| 10 | **hsa-miR-598** | 2,411.82 | **hsa-miR-16-5p** | 2,361.77 |
| 11 | hsa-miR-1183 | 2,368.62 | hsa-miR-130a-3p | 2,077.57 |
| 12 | hsa-let-7b-5p | 2,116.64 | hsa-miR-106a-5p+hsa-miR-17-5p | 2,008.97 |
| 13 | **hsa-miR-630** | 2,087.84 | **hsa-miR-4286** | 1,701.91 |
| 14 | hsa-miR-4516 | 2,015.85 | hsa-miR-93-5p | 1,692.11 |
| 15 | hsa-miR-4488 | 2,008.65 | **hsa-let-7g-5p** | 1,587.58 |
| 16 | hsa-miR-548al | 1,943.86 | hsa-miR-106b-5p | 1,561.45 |
| 17 | hsa-miR-199a-3p+hsa-miR-199b-3p | 1,936.66 | hsa-miR-20a-5p+hsa-miR-20b-5p | 1,545.11 |
| 18 | **hsa-miR-29b-3p** | 1,699.07 | **hsa-miR-630** | 1,528.78 |
| 19 | **hsa-miR-145-5p** | 1,641.48 | hsa-miR-25-3p | 1,512.45 |
| 20 | hsa-miR-222-3p | 1,497.49 | hsa-miR-155-5p | 1,463.45 |
| 21 | **hsa-miR-100-5p** | 1,432.69 | **hsa-miR-29a-3p** | 1,463.45 |
| 22 | hsa-miR-495 | 1,396.7 | hsa-miR-19b-3p | 1,427.51 |
| 23 | **hsa-miR-29a-3p** | 1,360.7 | hsa-miR-15a-5p | 1,388.31 |
| 24 | hsa-miR-187-3p | 1,360.7 | **hsa-miR-598** | 1,270.72 |
| 25 | hsa-let-7i-5p | 1,346.3 | hsa-miR-378e | 1,260.92 |
| 26 | **hsa-let-7g-5p** | 1,331.9 | hsa-miR-191-5p | 1,189.05 |
| 27 | hsa-miR-518b | 1,317.5 | **hsa-miR-145-5p** | 1,051.85 |
| 28 | hsa-miR-4532 | 1,317.5 | **hsa-miR-4443** | 1,038.79 |
| 29 | **hsa-miR-16-5p** | 1,303.1 | hsa-miR-1260a | 1,009.39 |
| 30 | hsa-miR-302d-3p | 1,259.91 | hsa-miR-99b-5p | 1,009.39 |

miRNAs in boldface font were expressed at high levels in both MSC and HOS exosomes.
Abbreviations: HOS, human osteosarcoma cell; miRNAs, microRNAs; MSC, mesenchymal stem cell.

not seem to be important in stem cell homing for tissue regeneration because the injection of MSC exosomes into CD9$^{-/-}$ mice rescued the retardation of fracture healing. These results suggest that the reduction and/or dysfunction of exosomes are at least one of the causes of delayed-fracture healing in CD9$^{-/-}$ mice.

The therapeutic potential of MSCs continues to receive widespread attention [10]. We therefore focused on the therapeutic implications of MSC exosomes as a novel paracrine factor secreted by MSCs. The present study showed that CM and MSC exosomes accelerate fracture healing. However, exosomes derived from HOS, an osteosarcoma cell line, did not have this capability. Previously, it was reported that serum-free conditioned medium derived from human MSCs accelerates callus formation in a mouse distraction osteogenesis model. MCP-1/-3 and interleukin-3 (IL-3)/IL-6 in CM recruit bone marrow stromal cells, mature endothelial cells, and progenitor cells, and induce angiogenesis and osteogenic differentiation [14]. Another group also reported that MCP-1 and SDF-1 promote endochondral bone repair by recruiting MSCs to the site of injury [12, 13]. These studies demonstrated the functional capabilities of MCP-1 and SDF-1 using neutralizing antibodies in MCP-1$^{-/-}$ and SDF-1$^{+/-}$ mouse models. However, our data revealed that the MCP-1, MCP-3, and SDF-1 concentrations in MSC exosomes were significantly lower than in CM and/or CM-Exo. Interestingly, although CM-Exo was not able to promote fracture healing, the levels of several angiogenic factors, SDF-1, MCP-1, and MCP-3, in CM-Exo were higher than in MSC exosomes. Notably, MCP-1 levels were markedly low in HOS exosomes compared with MSC exosomes. Angiogenesis also plays an important role in fracture healing [46]. CM contains high levels of angiogenic factors such as VEGF and IL-6 and enhances bone ingrowth and fracture healing by stimulating endothelial cells [47]. However, as we previously reported, although VEGF and IL-6 levels in MSC exosomes are low compared with CM and CM-Exo, MSC

 

**Table 2.** miRNA levels in MSC exosomes relative to HOS exosomes

| miRNAs | Ratio, MSC exo/ HOS exo | MSC exo | HOS exo |
|---|---|---|---|
| hsa-miR-338-3p[a] | 5.51 | 1,223.91 | 222.13 |
| hsa-miR-548aa[a] | 5.06 | 892.73 | 176.4 |
| **hsa-miR-4532** | 4.86 | **1,317.50** | 271.13 |
| hsa-miR-376a-3p | 4.64 | 1,015.12 | 218.86 |
| **hsa-miR-125b-5p** | 4.63 | **11,785.52** | 2,547.97 |
| **hsa-miR-4516** | 4.54 | **2,015.85** | 444.26 |
| hsa-miR-136-5p | 4.33 | 410.37 | 94.73 |
| hsa-miR-125a-3p | 4.01 | 575.96 | 143.73 |
| hsa-miR-34a-5p | 3.65 | 763.14 | 209.06 |
| hsa-miR-671-3p | 3.60 | 223.18 | 62.07 |
| hsa-miR-376c | 3.56 | 604.75 | 169.86 |
| hsa-miR-300 | 3.43 | 302.38 | 88.2 |
| hsa-miR-617 | 3.43 | 201.58 | 58.8 |
| hsa-miR-4521 | 3.42 | 323.98 | 94.73 |
| hsa-miR-217 | 3.41 | 244.78 | 71.87 |
| hsa-miR-5480-3p | 3.31 | 367.17 | 111.07 |
| hsa-miR-3161 | 3.27 | 331.18 | 101.27 |
| hsa-miR-548q | 3.26 | 511.16 | 156.8 |
| hsa-miR-33b-5p | 3.25 | 424.77 | 130.66 |
| hsa-miR-1269a | 3.23 | 316.78 | 98 |
| hsa-miR-337-5p | 3.22 | 410.37 | 127.4 |
| hsa-miR-1291 | 3.21 | 367.17 | 114.33 |
| hsa-miR-1295a | 3.21 | 230.38 | 71.87 |
| hsa-miR-487a | 3.19 | 302.38 | 94.73 |
| hsa-miR-939 | 3.19 | 395.97 | 124.13 |
| hsa-miR-551b-3p | 3.14 | 266.38 | 84.93 |
| hsa-miR-3180 | 3.09 | 403.17 | 130.66 |
| hsa-miR-371a-5p | 3.09 | 251.98 | 81.67 |
| hsa-miR-1269b | 3.06 | 179.99 | 58.8 |
| hsa-miR-133a | 3.03 | 237.58 | 78.4 |
| hsa-miR-298 | 3.00 | 381.57 | 127.4 |

Differential miRNA levels (at least 3.0-fold difference) are shown as the ratio of levels in MSC exosomes relative to those in HOS exosomes. Absolute counts of miRNA levels in MSC and HOS exosomes are presented in columns three and four. miRNAs in bold boldface font were the top 30 most highly expressed miRNAs in MSC exosomes.
[a]These miRNAs were present at ratios 2.5-fold greater than the ratio of MSC-exo/CM-exo.
Abbreviations: Exo, exosomes; HOS, human osteosarcoma cell; miRNAs, microRNAs; MSC, mesenchymal stem cell.

exosomes induce angiogenesis to a greater extent [36]. These results suggest that the acceleration of fracture healing by MSC exosomes is not solely attributable to MCP-1, -3, SDF-1, and angiogenic factors. Exosomes contain mRNAs and miRNAs, as well as cytokines, and functional RNAs can be transferred from one cell to another via the exosome [48–50]. We previously identified miRNAs in MSC exosomes, CM, and CM-Exo. Among them, miR-21, an antiapoptotic miRNA, was most abundant in MSC exosomes and MSC-CM [36]. MiR-21 promotes osteogenic differentiation of MSCs [51, 52], and local injection of miR-21 overexpressing MSCs promotes fracture healing in a rat model [53]. Our analysis revealed that the levels of miR-21 were high in both HOS and MSC exosomes. Many highly expressed miRNAs in MSC exosomes were similar to those in HOS exosomes. Highly expressed miRNAs are common in exosomes from many different cells [36, 54, 55]. However, among the top 30 most highly expressed miRNAs in MSC exosomes, several, such as miR-4532, miR-125b-5p, and miR-338-3p, were more abundant or were significantly differentially expressed in MSC exosomes relative to HOS exosomes or CM-Exo. These miRNAs are still unknown to be involved in tissue regeneration, including fracture healing. Thus, a future study probably should be more focused on stem cell-specific miRNA. Although it is difficult to determine which miRNA contributed most to the acceleration of fracture healing by MSC exosomes, miRNA in MSC exosomes may play a critical role in tissue regeneration as a unique set of miRNA. The acceleration of fracture healing by MSC exosomes may not only be related to the recruitment of stem cells or progenitor cells by cytokines such as MCP-1 and SDF-1, but also the induction of osteogenesis and angiogenesis, which is at least in part mediated by miRNAs in exosomes. MiRNAs control tissue development and homeostasis through fine-tuning gene expression [56]. MSC-exosome miRNAs might contribute to the dynamics of tissue regeneration by influencing the microenvironment at the repair site. Furthermore, it was recently reported that exosomes are effective carriers of siRNA and miRNA [57–59]. Thus, engineered exosomes may be a potentially efficient RNA delivery system for the treatment of various diseases and tissue regeneration, and MSC exosomes may provide a useful tool to uncover new mechanisms involved in tissue repair.

## Conclusion

This study demonstrated that MSC-derived exosomes play an important role in fracture healing through facilitation of endochondral ossification. The injection of exosomes rescued the retardation of fracture healing in $CD9^{-/-}$ mice, whereas exosome-free conditioned culture medium (CM-Exo) failed to accelerate fracture repair. Thus, we conclude that exosomes are a novel component of the paracrine effect of MSCs, which modulate fracture healing. Exosomes may contribute significantly to the mechanism of tissue regeneration by MSC transplantation.

## Acknowledgments

We thank T. Miyata for excellent technical support and M. Miyaki for help in the statistical analysis. This research was supported by MEXT/JPS KAKENHI Grant-in-Aid for Scientific Research (A) 21249079 (M.O.); EXT/JPS KAKENHI Grant-in-Aid for Scientific Research (B) 15H04959 (S.M.); and Young Scientists (A) Grant 24689057 (S.M.).

## Author Contributions

T.F.: conception and design, collection and/or assembly of data, data analysis and interpretation, manuscript writing, final approval of manuscript; S.M.: conception and design, data analysis and interpretation, manuscript writing, final approval of manuscript; H.I.: collection and/or assembly of data, final approval of manuscript; T.O. and Y.K.: collection and/or assembly of data,

manuscript writing, final approval of manuscript; N.K.: collection and/or assembly of data, data analysis and interpretation, final approval of manuscript; K.M.: provision of study material or patients, data analysis and interpretation, final approval of manuscript; Y.H.: data analysis and interpretation, manuscript writing, final approval of manuscript; M.O.: collection and/or assembly of data, data analysis and interpretation, manuscript writing, final approval of manuscript.

## Disclosure of Potential Conflicts of Interest

The authors indicated no potential conflicts of interest.

## References


**1** Rhinelander FW, Baragry R. Microangiography in bone healing. I. Undisplaced closed fractures. J Bone Joint Surg 1962;44-A: 1273–1298.

**2** Enneking WF, Eady JL, Burchardt H. Autogenous cortical bone grafts in the reconstruction of segmental skeletal defects. J Bone Joint Surg Am 1980;62:1039–1058.

**3** Kodama A, Kamei N, Kamei G et al. In vivo bioluminescence imaging of transplanted bone marrow mesenchymal stromal cells using a magnetic delivery system in a rat fracture model. J Bone Joint Surg Br 2012;94:998–1006.

**4** Granero-Moltó F, Myers TJ, Weis JA et al. Mesenchymal stem cells expressing insulin-like growth factor-I (MSCIGF) promote fracture healing and restore new bone formation in Irs1 knockout mice: Analyses of MSCIGF autocrine and paracrine regenerative effects. Stem Cells 2011;29:1537–1548.

**5** Pittenger MF, Martin BJ. Mesenchymal stem cells and their potential as cardiac therapeutics. Circ Res 2004;95:9–20.

**6** Watson L, Elliman SJ, Coleman CM. From isolation to implantation: A concise review of mesenchymal stem cell therapy in bone fracture repair. Stem Cell Res Ther 2014;5:51.

**7** Caplan AI, Dennis JE. Mesenchymal stem cells as trophic mediators. J Cell Biochem 2006;98:1076–1084.

**8** Granero-Moltó F, Weis JA, Miga MI et al. Regenerative effects of transplanted mesenchymal stem cells in fracture healing. Stem Cells 2009;27:1887–1898.

**9** Gerstenfeld LC, Cullinane DM, Barnes GL et al. Fracture healing as a post-natal developmental process: Molecular, spatial, and temporal aspects of its regulation. J Cell Biochem 2003; 88:873–884.

**10** Liang X, Ding Y, Zhang Y et al. Paracrine mechanisms of mesenchymal stem cell-based therapy: Current status and perspectives. Cell Transplant 2014;23:1045–1059.

**11** Toupadakis CA, Wong A, Genetos DC et al. Long-term administration of AMD3100, an antagonist of SDF-1/CXCR4 signaling, alters fracture repair. J Orthopaedic Res 2012;30: 111853–1859.

**12** Ishikawa M, Ito H, Kitaori T et al. MCP/CCR2 signaling is essential for recruitment of mesenchymal progenitor cells during the early phase of fracture healing. PLoS One 2014;9:e104954.

**13** Kitaori T, Ito H, Schwarz EM et al. Stromal cell-derived factor 1/CXCR4 signaling is critical for the recruitment of mesenchymal stem cells to the fracture site during skeletal repair in a mouse model. Arthritis Rheum 2009;60:813–823.

**14** Ando Y, Matsubara K, Ishikawa J et al. Stem cell-conditioned medium accelerates distraction osteogenesis through multiple regenerative mechanisms. Bone 2014;61:82–90.

**15** Mu J, Zhuang X, Wang Q et al. Interspecies communication between plant and mouse gut host cells through edible plant derived exosome-like nanoparticles. Mol Nutr Food Res 2014;58:1561–1573.

**16** Ludwig AK, Giebel B. Exosomes: Small vesicles participating in intercellular communication. Int J Biochem Cell Biol 2012;44: 11–15.

**17** Pan BT, Johnstone RM. Fate of the transferrin receptor during maturation of sheep reticulocytes in vitro: Selective externalization of the receptor. Cell 1983;33:967–978.

**18** Johnstone RM. Exosomes biological significance: A concise review. Blood Cells Mol Dis 2006;36:315–321.

**19** Zakharova L, Svetlova M, Fomina AF. T cell exosomes induce cholesterol accumulation in human monocytes via phosphatidylserine receptor. J Cell Physiol 2007;212: 174–181.

**20** Théry C, Ostrowski M, Segura E. Membrane vesicles as conveyors of immune responses. Nat Rev Immunol 2009;9:581–593.

**21** Mathivanan S, Ji H, Simpson RJ. Exosomes: Extracellular organelles important in intercellular communication. J Proteomics 2010; 73:1907–1920.

**22** Iwasaki T, Takeda Y, Maruyama K et al. Deletion of tetraspanin CD9 diminishes lymphangiogenesis in vivo and in vitro. J Biol Chem 2013;288:2118–2131.

**23** Kamisasanuki T, Tokushige S, Terasaki H et al. Targeting CD9 produces stimulus-independent antiangiogenic effects predominantly in activated endothelial cells during angiogenesis: A novel antiangiogenic therapy. Biochem Biophys Res Commun 2011; 413:128–135.

**24** Qi JC, Wang J, Mandadi S et al. Human and mouse mast cells use the tetraspanin CD9 as an alternate interleukin-16 receptor. Blood 2006;107:135–142.

**25** Record M. Intercellular communication by exosomes in placenta: A possible role in cell fusion? Placenta 2014;35:297–302.

**26** Dou C, Li J, Kang F et al. Dual effect of cyanidin on RANKL-induced differentiation and fusion of osteoclasts. J Cell Physiol 2016;231: 558–567.

**27** Tachibana I, Hemler ME. Role of transmembrane 4 superfamily (TM4SF) proteins CD9 and CD81 in muscle cell fusion and myotube maintenance. J Cell Biol 1999;146: 893–904.

**28** Miyado K, Yamada G, Yamada S et al. Requirement of CD9 on the egg plasma membrane for fertilization. Science 2000;287: 321–324.

**29** Ishii M, Iwai K, Koike M et al. RANKL-induced expression of tetraspanin CD9 in lipid raft membrane microdomain is essential for cell fusion during osteoclastogenesis. J Bone Miner Res 2006;21:6965–976.

**30** Yi T, Kim HJ, Cho JY et al. Tetraspanin CD9 regulates osteoclastogenesis via regulation of p44/42 MAPK activity. Biochem Biophys Res Commun 2006;347:178–184.

**31** Miyado K, Yoshida K, Yamagata K et al. The fusing ability of sperm is bestowed by CD9-containing vesicles released from eggs in mice. Proc Natl Acad Sci USA 2008;105: 12921–12926.

**32** Chairoungdua A, Smith DL, Pochard P et al. Exosome release of $\beta$-catenin: A novel mechanism that antagonizes Wnt signaling. J Cell Biol 2010;190:1079–1091.

**33** Bruno S, Grange C, Deregibus MC et al. Mesenchymal stem cell-derived microvesicles protect against acute tubular injury. J Am Soc Nephrol 2009;20:1053–1067.

**34** Herrera MB, Fonsato V, Gatti S et al. Human liver stem cell-derived microvesicles accelerate hepatic regeneration in hepatectomized rats. J Cell Mol Med 2010;14(6b): 1605–1618.

**35** Lai RC, Arslan F, Lee MM et al. Exosome secreted by MSC reduces myocardial ischemia/reperfusion injury. Stem Cell Res (Amst) 2010;4:214–222.

**36** Nakamura Y, Miyaki S, Ishitobi H et al. Mesenchymal-stem-cell-derived exosomes accelerate skeletal muscle regeneration. FEBS Lett 2015;589:1257–1265.

**37** Maes C, Coenegrachts L, Stockmans I et al. Placental growth factor mediates mesenchymal cell development, cartilage turnover, and bone remodeling during fracture repair. J Clin Invest 2006;116:1230–1242.

**38** Oetgen ME, Merrell GA, Troiano NW et al. Development of a femoral non-union model in the mouse. Injury 2008;39:1119–1126.

**39** Ogura T. Nanoscale analysis of unstained biological specimens in water without radiation damage using high-resolution frequency transmission electric-field system based on FE-SEM. Biochem Biophys Res Commun 2015;459: 521–528.

**40** Zhang J, Dong J, Gu H et al. CD9 is critical for cutaneous wound healing through JNK signaling. J Invest Dermatol 2012;132: 226–236.

**41** Charrin S, Latil M, Soave S et al. Normal muscle regeneration requires tight control of muscle cell fusion by tetraspanins CD9 and CD81. Nat Commun 2013;4:1674.

**42** Kawano N, Miyado K, Yoshii N et al. Absence of CD9 reduces endometrial VEGF secretion and impairs uterine repair after parturition. Sci Rep 2014;4:4701.

**43** Takeda Y, Tachibana I, Miyado K et al. Tetraspanins CD9 and CD81 function to prevent the fusion of mononuclear phagocytes. J Cell Biol 2003;161:945–956.

**44** Leung KT, Chan KY, Ng PC et al. The tetraspanin CD9 regulates migration, adhesion, and homing of human cord blood CD34+ hematopoietic stem and progenitor cells. Blood 2011; 117:1840–1850.


 

**45** Brzoska E, Kowalski K, Markowska-Zagrajek A et al. Sdf-1 (CXCL12) induces CD9 expression in stem cells engaged in muscle regeneration. Stem Cell Res Ther 2015;6: 46.

**46** Saran U, Gemini Piperni S, Chatterjee S. Role of angiogenesis in bone repair. Arch Biochem Biophys 2014;561:109–117.

**47** Wang CY, Yang HB, Hsu HS et al. Mesenchymal stem cell-conditioned medium facilitates angiogenesis and fracture healing in diabetic rats. J Tissue Eng Regen Med 2012;6: 559–569.

**48** Valadi H, Ekström K, Bossios A et al. Exosome-mediated transfer of mRNAs and microRNAs is a novel mechanism of genetic exchange between cells. Nat Cell Biol 2007;9: 654–659.

**49** Zhang Y, Liu D, Chen X et al. Secreted monocytic miR-150 enhances targeted endothelial cell migration. Mol Cell 2010;39:133–144.

**50** Kosaka N, Iguchi H, Yoshioka Y et al. Secretory mechanisms and intercellular transfer of microRNAs in living cells. J Biol Chem 2010; 285:17442–17452.

**51** Li H, Yang F, Wang Z et al. MicroRNA-21 promotes osteogenic differentiation by targeting small mothers against decapentaplegic 7. Mol Med Rep 2015;12:1561–1567.

**52** Meng YB, Li X, Li ZY et al. microRNA-21 promotes osteogenic differentiation of mesenchymal stem cells by the PI3K/beta-catenin pathway. J Orthop Res 2015;33:7957–964.

**53** Sun Y, Xu L, Huang S et al. mir-21 overexpressing mesenchymal stem cells accelerate fracture healing in a rat closed femur fracture model. BioMed Res Int 2015;2015:412327.

**54** Baglio SR, Rooijers K, Koppers-Lalic D et al. Human bone marrow- and adipose-mesenchymal stem cells secrete exosomes enriched in distinctive miRNA and tRNA species. Stem Cell Res Ther 2015;6:127.

**55** Kato T, Miyaki S, Ishitobi H et al. Exosomes from IL-1$\beta$ stimulated synovial fibroblasts induce osteoarthritic changes in articular chondrocytes. Arthritis Res Ther 2014;16:R163.

**56** Miyaki S, Asahara H. Macro view of microRNA function in osteoarthritis. Nat Rev Rheumatol 2012;8:543–552.

**57** Alvarez-Erviti L, Seow Y, Yin H et al. Delivery of siRNA to the mouse brain by systemic injection of targeted exosomes. Nat Biotechnol 2011;29:341–345.

**58** Ohno S, Takanashi M, Sudo K et al. Systemically injected exosomes targeted to EGFR deliver antitumor microRNA to breast cancer cells. Mol Ther 2013;21:1185–191.

**59** Shimbo K, Miyaki S, Ishitobi H et al. Exosome-formed synthetic microRNA-143 is transferred to osteosarcoma cells and inhibits their migration. Biochem Biophys Res Commun 2014;445:381–387.

See www.StemCellsTM.com for supporting information available online.